Out-of-plane shear flow effects on fast magnetic reconnection in a two-dimensional hybrid simulation model*

Wang Lin(王 琳)[a)b)], Wang Xian-Qu(王先驱)[c)], Wang Xiao-Gang(王晓钢)[c)†], and Liu Yue(刘 悦)[a)]

[a)] *MOE Key Laboratory of Materials Modification by Beams and School of Physics & Optoelectronic Technology, Dalian University of Technology, Dalian* 116024, *China*

[b)] *School of Information Science & Engineering, Dalian Polytechnic University, Dalian* 116034, *China*

[c)] *State Key Laboratory of Nuclear Physics & Technology and School of Physics, Peking University, Beijing* 100871, *China*

(Received 30 May 2013; revised manuscript received 4 July 2013; published online 10 December 2013)

The effects of out-of-plane shear flows on fast magnetic reconnection are numerically investigated by a two-dimensional (2D) hybrid model in an initial Harris sheet equilibrium with flows. The equilibrium and driven shear flows out of the 2D reconnection plane with symmetric and antisymmetric profiles respectively are used in the simulation. It is found that the out-of-plane flows with shears in-plane can change the quadrupolar structure of the out-of-plane magnetic field and, therefore, modify the growth rate of magnetic reconnection. Furthermore, the driven flow varying along the anti-parallel magnetic field can either enhance or reduce the reconnection rate as the direction of flow changes. Secondary islands are also generated in the process with converting the initial X-point into an O-point.

Keywords: out-of-plane magnetic field, shear flow, magnetic reconnection, Hall effects

PACS: 52.35.Vd, 52.30.–q, 94.30.–d, 96.60.lv **DOI:** 10.1088/1674-1056/23/2/025203

1. Introduction

Magnetic reconnection, a process of magnetic flux merging, cutting, and reconnecting, is a fundamental course in laboratory and space plasma physics.[1,2] During magnetic reconnection, a large amount of stored magnetic energy in a plasma is rapidly released and converted into plasma particle acceleration and heating.[2] It, thus, plays a critical role in fast energy transformation events, such as solar flares, coronal mass ejections, interaction of solar winds with the geomagnetosphere, and the formation of stars.[3] Due to its significance, magnetic reconnection has been extensively investigated in various aspects during recent decades; particularly for fast growth, geometry features, and collisionless effects such as Hall effect.[1–10]

Shear flows are easily generated in space and fusion plasmas. In magnetically confined fusion devices, it is found that in experiments and numerical simulations, shear flows (i.e., differential plasma rotations) can considerably affect magnetohydrodynamics (MHD) processes, such as tearing modes, error field lock modes, and resistive wall modes, as well as singular current layer formation and Alfven resonance generation.[11–21] On the other hand, in space plasmas the solar wind blowing on the magnetosphere often creates a velocity shear across the magnetopause.[22] In particular, transient strong shear flow events with a substantial north-southward electric field and energetic ion beams, as well as field-aligned currents, are also observed at the boundary of the pre-midnight plasma sheet.[23] Numerically, the effect of shear flows on the structure of the reconnection layer at the flank magnetopause has also been studied by one-dimensional (1D) hybrid and two-dimensional (2D) MHD simulations.[24,25] The reconnection layer structure with an in-plane shear flow perpendicular to the anti-parallel magnetic field component was also investigated for the 1D MHD Riemann problem.[26] It was discovered that such shear flows resulted in structures associated with MHD discontinuities, which is drastically different from that without shear flows or with shear flows parallel to the initial magnetic field.

In addition to the in-plane shear flows studied previously, out-of-plane "toroidal" shear flows have also recently been considered.[27,28] It was revealed that the out-of-plane shear flows generated a bipolar or quadrupolar structure of the out-of-plane magnetic field perturbation. Moreover, it was also demonstrated that reconnection processes, particularly in the collision-free regime, were in certain cases dominated by the out-of-plane shear flow in Hall MHD simulations. Then, the effects had a significant influence on the theory and observations of fast magnetic reconnection. Nevertheless, Hall MHD is a simplified two-fluid model and, in the ion inertial region where Hall MHD is adopted mostly, the kinetic effect of ion dynamics should be taken into account.

Hybrid simulations codes, by taking electrons as a massless fluid approximately but keeping full ion dynamics in a particle-in-cell (PIC) treatment, have been developed to study collisionless magnetic reconnection.[29–32] It has been demonstrated that the hybrid model is a powerful tool in the regime

*Project supported by the National Natural Science Foundation of China (Grant Nos. 10935004, 1126114032, 10778613, 10575018, 40731056, 10975012, and 11261140326).

†Corresponding author. E-mail: xgwang@pku.edu.cn

© 2014 Chinese Physical Society and IOP Publishing Ltd

on a time scale of $\omega \lesssim \Omega_0$ and spatial scale of $k\rho_0 \lesssim 1$, where ω is the wave frequency of the perturbation, k is the wave number, and Ω_0 and ρ_0 are the gyro-frequency and gyro-radius of ions, respectively.[32] Thus, in this paper, we conduct a 2D hybrid simulation to further study the effect of the out-of-plane shear flows on fast magnetic reconnection. The simulation model with initial conditions is given in Section 2. The simulation results of the effects of the flows varying across the current sheet and in the anti-parallel magnetic field directions are presented in Sections 3 and 4, respectively. Finally, this paper concludes with a discussion and summary in Section 5.

2. Model and initial conditions

We will first briefly describe the model, which is similar to that in Refs. [27]–[30], that we have applied to our hybrid simulation. The equation for the ion motion is written in the form of[30]

$$\frac{\mathrm{d}\boldsymbol{V}_\mathrm{i}}{\mathrm{d}t} = \frac{e}{m_\mathrm{i}}\left(\boldsymbol{E} + \frac{1}{c}\boldsymbol{V}_\mathrm{i}\times\boldsymbol{B}\right) - \nu\left(\boldsymbol{u}_\mathrm{i} - \boldsymbol{u}_\mathrm{e}\right), \tag{1}$$

to advance individual particles by the Lorentz force with Krook collision on the bulk flow. Here $\boldsymbol{V}_\mathrm{i}$, m_i, e, $\boldsymbol{E}$, $\boldsymbol{B}$, and c are the velocity and mass of an individual ion particle, the element charge, the electric and magnetic fields, and the speed of light, respectively. ν is the collision frequency between ions and electrons, $\boldsymbol{u}_\mathrm{i}$ and $\boldsymbol{u}_\mathrm{e}$ are the ion and electron bulk flow velocities, respectively. To bring about the resistivity effect, the collision frequency is applied to the bulk flow rather than to individual particles with respect to the electron fluid. It is notable that $\boldsymbol{V}$ is used here for the individual particle velocity, while $\boldsymbol{u}$ is for the flow velocity. The massless electron momentum equation is given by

$$\frac{e}{m_\mathrm{i}}\left(\boldsymbol{E} + \frac{1}{c}\boldsymbol{u}_\mathrm{e}\times\boldsymbol{B}\right) + \nu\left(\boldsymbol{u}_\mathrm{e} - \boldsymbol{u}_\mathrm{i}\right) = 0, \tag{2}$$

which is obtained from the electron fluid equations by ignoring the pressure. The electron flow velocities can also be calculated by Ampere's law

$$\nabla\times\boldsymbol{B} = \frac{4\pi}{c}ne\left(\boldsymbol{u}_\mathrm{i} - \boldsymbol{u}_\mathrm{e}\right), \tag{3}$$

where n is the number density of the ions with its maximum n_0 and the high frequency displacement current effect is neglected. In addition, Faraday's law

$$\nabla\times\boldsymbol{E} = -\frac{1}{c}\frac{\partial\boldsymbol{B}}{\partial t} \tag{4}$$

is used for updating the magnetic field.

The dimensionless equations for hybrid simulation are, thus, written as

$$\frac{\mathrm{d}\boldsymbol{V}_\mathrm{i}}{\mathrm{d}t} = \boldsymbol{E} + \boldsymbol{V}_\mathrm{i}\times\boldsymbol{B} - \bar{\nu}\left(\boldsymbol{u}_\mathrm{i} - \boldsymbol{u}_\mathrm{e}\right), \tag{5}$$

$$\boldsymbol{E} = -\boldsymbol{u}_\mathrm{e}\times\boldsymbol{B} - \bar{\nu}\left(\boldsymbol{u}_\mathrm{e} - \boldsymbol{u}_\mathrm{i}\right), \tag{6}$$

$$\boldsymbol{u}_\mathrm{e} = \boldsymbol{u}_\mathrm{i} - \frac{\nabla\times\boldsymbol{B}}{\bar{n}}, \tag{7}$$

$$\frac{\partial\boldsymbol{B}}{\partial t} = -\nabla\times\boldsymbol{E}. \tag{8}$$

Here, the length is scaled by the ion inertial length $\lambda_0 = c/\omega_{\mathrm{pi}0}$, $\omega_{\mathrm{pi}0} = \left(4\pi n_0 e^2/m_\mathrm{i}\right)^{1/2}$ is the ion plasma frequency, and time is scaled by Ω_0^{-1}, where $\Omega_0 = eB_0/m_\mathrm{i}c$ is the ion gyro-frequency with B_0 being the asymptotic field. Then, both velocities $\boldsymbol{V}$ and $\boldsymbol{u}$ are scaled by the Alfvén velocity $V_\mathrm{A}=\lambda_0\Omega_0$ and, therefore, clearly the Alfvén time $\tau_\mathrm{A} \equiv \lambda_0/V_\mathrm{A} = \Omega_0^{-1}$. The electric field $\boldsymbol{E}$ and the magnetic field $\boldsymbol{B}$ are scaled by $V_\mathrm{A}B_0/c$ and B_0, respectively, while $\bar{n}=n/n_0$, and $\bar{\nu}=\nu/\Omega_0$. By substituting Eqs. (6) and (7) into Eq. (5), we obtain

$$\frac{\mathrm{d}\boldsymbol{V}_\mathrm{i}}{\mathrm{d}t} = \boldsymbol{E}_\mathrm{p} + \boldsymbol{V}_\mathrm{i}\times\boldsymbol{B}, \tag{9}$$

with

$$\boldsymbol{E}_\mathrm{p} = -\boldsymbol{u}_\mathrm{e}\times\boldsymbol{B} = \left(\frac{\nabla\times\boldsymbol{B}}{\bar{n}} - \boldsymbol{u}_\mathrm{i}\right)\times\boldsymbol{B}. \tag{10}$$

The simulation domain is a rectangular box, $-L_x/2 \le x \le L_x/2$, $-L_z/2 \le x \le L_z/2$, in the x–z plane with a size of $L_x \times L_z = 100 \times 50$ (scaled in λ_0). It is divided into 100×100 grids uniformly with $\Delta x = 2\Delta z = 1$.

The initial equilibrium is a 2D Harris current sheet symmetrically distributed in the $z = 0$ plane with a magnetic field of

$$B_{x0}(z) = B_0\tanh(z/L_0), \tag{11}$$

where L_0 is the half width of the Harris sheet. For fast reconnection, we make an assumption of the thin current sheet with $L_0 = 2$ in the simulation. The initial ion number density is given by

$$\bar{n}_0 = \frac{n(t=0)}{n_0} = 1 + \left(\beta_0\cosh^2\left(z/L_0\right)\right)^{-1}. \tag{12}$$

Here, we take the asymptotic ion number density $n_0 = 50$ per cell, and the asymptotic plasma beta $\beta_0 = 0.1$. A localized resistivity is used and given by

$$\bar{\nu} = \bar{\nu}_0\exp\left(-(x^2+z^2)/\lambda_0^2\right), \tag{13}$$

to trigger reconnection , where $\bar{\nu}_0 = 1.5$.[30] Also, the initial ion temperature T_i is assumed to satisfy the equilibrium condition

$$\bar{n}_0(z)T_{\mathrm{i}0}(z) + \frac{1}{2}\bar{n}_0(z)u_{\mathrm{i}z0}^2(z) + \frac{B_{x0}^2(z)}{8\pi} = \text{const.} \tag{14}$$

The open boundary condition is imposed on the boundaries of $x = \pm L_x/2$, while the fixed conditions are applied to the boundaries of $z = \pm L_z/2$, with perturbations of both magnetic field component B_z and inflow velocity $u_{\mathrm{i}z}$ vanished for free magnetic reconnection.

3. Effects of flows with shear in z direction

As in Refs. [27] and [28], we first use the out-of-plane shear flow varying in the direction across the current sheet in the initial equilibrium, that is, the flow shear (its magnitude variation) is set to be along the z axis, which is the same as the initial magnetic field shear, and satisfies the Harris sheet equilibrium in 2D geometry. We then discuss the flow effects on reconnection for anti-symmetric and symmetric cases separately.

3.1. Effect of symmetric flows varied in the z direction (Case I)

In a way that is similar to that in Ref. [27], we introduce a symmetric out-of-plane shear flow profile, shown in Fig. 1(a), as

$$u_{\mathrm{i}y0}(z) = \begin{cases} U_0\left[1+\cos\left(\pi z/L_{\mathrm{S}}\right)\right], & -L_{\mathrm{S}} < z < L_{\mathrm{S}}, \\ 0, & \text{otherwise}, \end{cases} \tag{15}$$

where the flow shear length L_{S} is taken to be the same as the half width of the current sheet, that is, $L_{\mathrm{S}} = L_0 = 2$, and the shear flow strength U_0 is assumed to be $0.3V_{\mathrm{A}}$.

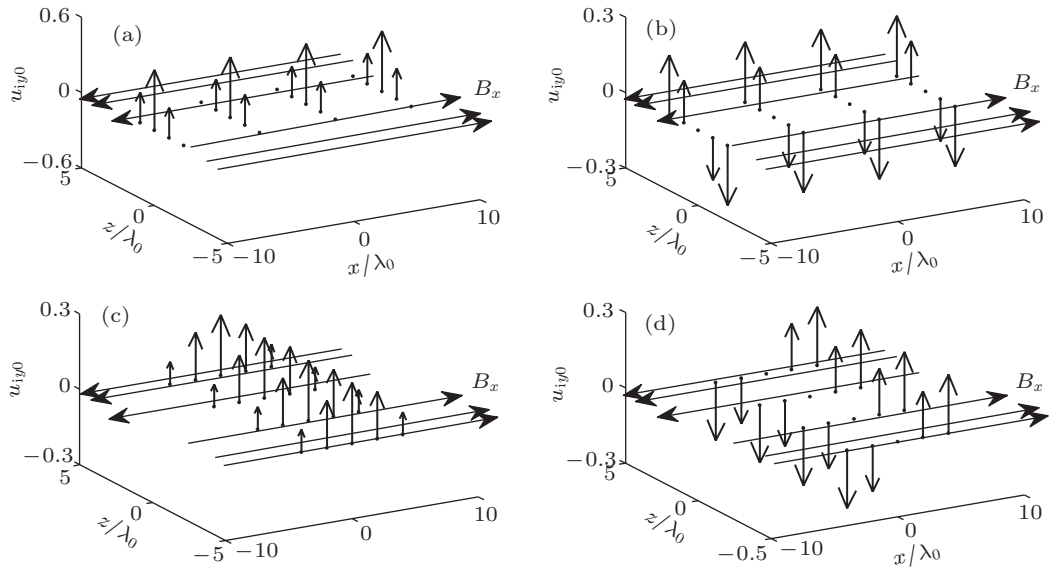


Fig. 1. Profiles of the out-of-plane shear flows applied, with (a) the symmetric (Case I) and (b) antisymmetric (Case II) flows varying in the z direction, and (c) the symmetric (Case III) and (d) antisymmetric (Case IV) flows varying in the x direction.

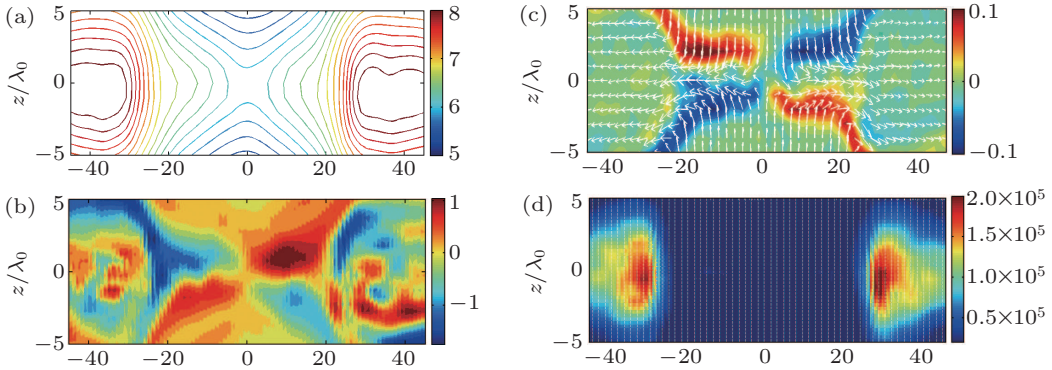


Fig. 2. (color online) Effects of the shear flow given by Eq. (15) with $U_0 = 0.3V_{\mathrm{A}}$ and at $t = 115\tau_{\mathrm{A}}$. Panel (a) shows the configuration of the in-plane magnetic flux, panel (b) shows the distribution of the out-of-plane magnetic field B_y, panel (c) shows the distributions of the out-of-plane vorticity ω_y (in contours) and the in-plane flows $\boldsymbol{u}_x + \boldsymbol{u}_z$ (in arrows), and panel (d) shows the density of plasma.

Figure 2 shows the configuration of the magnetic flux (Fig. 2(a)), a color contour plot of the out-of-plane magnetic field component (Fig. 2(b)), and the corresponding out-of-plane vorticity $\omega_y(x,z) = \partial u_x/\partial z - \partial u_z/\partial x$ together with the in-plane flow pattern shown by arrows (Fig. 2(c)), and the plasma density distribution (Fig. 2(d)); all the above figures are plotted at $t = 115\tau_{\mathrm{A}}$ in the vicinity of the $\boldsymbol{X}$-point. It is well known that in 2D hybrid and Hall MHD models without the out-of-plane shear flow, quadrupolar structures of both out-of-plane components of magnetic field B_y and vorticity ω_y are generated by the Hall effect. In fact, the symmetric out-of-plane shear flow also induces a quadrupolar out-of-plane mag-

netic perturbation parallel or opposite to that generated by the Hall effect and, thus, strengthens or weakens the quadrupolar Hall field component. Consequently, however, the flow shear itself is reduced in the process as the quadrupolar pattern of the vortex ω_y is formed. Thus, the effect does not significantly affect the maximum of the growth rate but only accelerates or delays the moment when the maximum is reached. Then, the temporal evolution of the magnetic energy E_m and the reconnection rate, $\partial\psi/\partial t$, are shown in Figs. 3(a) and 3(b), respectively. It can be seen that the reconnection rates calculated respectively by the slope of the magnetic energy growth shown in Fig. 3(a) and by the maximum of $\partial\psi/\partial t$, are both about 0.08, that is, $\gamma \approx 0.08$, which is the same as, but being reached later than, that without the shear flow (U_0=0).

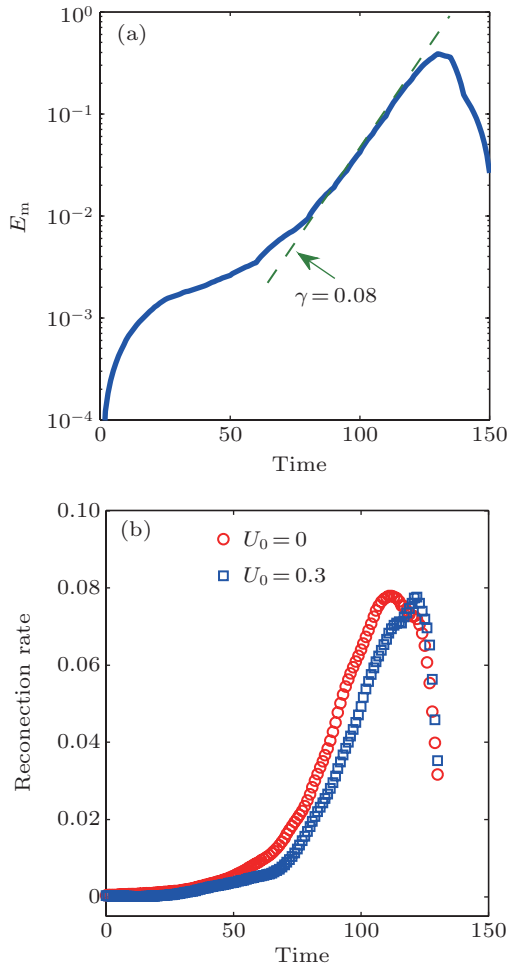


Fig. 3. (color online) Growth rates of reconnection in Case I. Panel (a) shows the temporal evolution of magnetic energy E_m, with the slope (dash line) representing the growth rate of $\gamma = \mathrm{d}(\ln E_m)/\mathrm{d}t \approx 0.08$, and panel (b) shows the temporal evolutions of $E_y = \partial\psi/\partial t$ for reconnection processes without the shear flow ($U_0 = 0$) and with shear flow ($U_0 = 0.3V_A$).

3.2. Effect of antisymmetric flow varying in z direction (Case II)

On the other hand, the antisymmetric out-of-plane shear flow profile shown also in Fig. 1(b) is introduced as

$$u_{iy0}(z) = \begin{cases} -U_0, & z \le -L_S, \\ U_0 \sin(\pi z/2L_S), & -L_S < z < L_S, \\ U_0, & z \ge L_S, \end{cases} \quad (16)$$

where L_S and U_0 are taken to be the same as those in Case I.

As in Fig. 2, the magnetic flux, the out-of-plane magnetic field component, the vortex of $\omega_y(x,z)$ together with the $u_x + u_z$ pattern, and the plasmas density distribution are plotted respectively in Fig. 4 at $t = 125\tau_A$, in the vicinity of the X-point. In contrast from Case I, although the quadrupolar pattern remains for the vortex ω_y, in this case, as shown in Fig. 4(c), an asymmetric structure of the out-of-plane magnetic field component B_y is found, as shown in Fig. 4(b). This indicates that the antisymmetric shear flow significantly reshapes the out-of-plane magnetic perturbation structure induced by the Hall effect in the reconnection process and probably changes the reconnection rate.

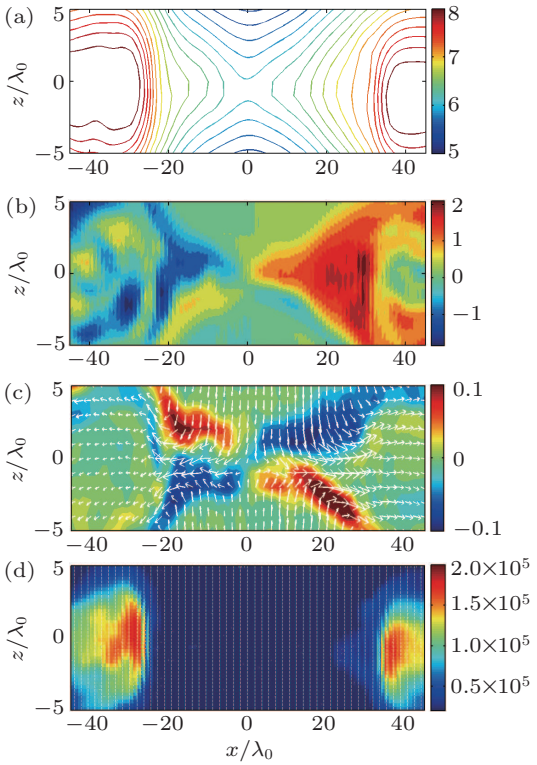


Fig. 4. (color online) Effects of the shear flows given by Eq. (16) with $U_0 = 0.3V_A$ and at $t = 125\tau_A$. Panel (a) shows the configuration of the in-plane magnetic flux, panel (b) showsthe distribution of the out-of-plane magnetic field B_y, panel (c) shows the distributions of the out-of-plane vorticity ω_y (in contours) and the in-plane flows $u_x + u_z$ (in arrows), and panel (d) shows the density of plasma.

The temporal evolutions of the magnetic energy E_m, together with the reconnection rate, $\partial\psi/\partial t$, are then shown in Fig. 5. It is found that the reconnection rate is approximately $\gamma \approx 0.07$ in this case, which is less than that without the shear flow ($\gamma = 0.08$ for U_0=0, as in Fig. 5(b)).

Furthermore, the quadrupolar structure of out-of-plane magnetic field has been taken as an important signature of fast magnetic reconnection.[33–37] It is, however, demonstrated in this case (Fig. 4(b)) that the quadrupolar pattern of the out-of-

plane magnetic field may be significantly distorted even in the collisionless regime if there exists an out-of-plane shear flow.

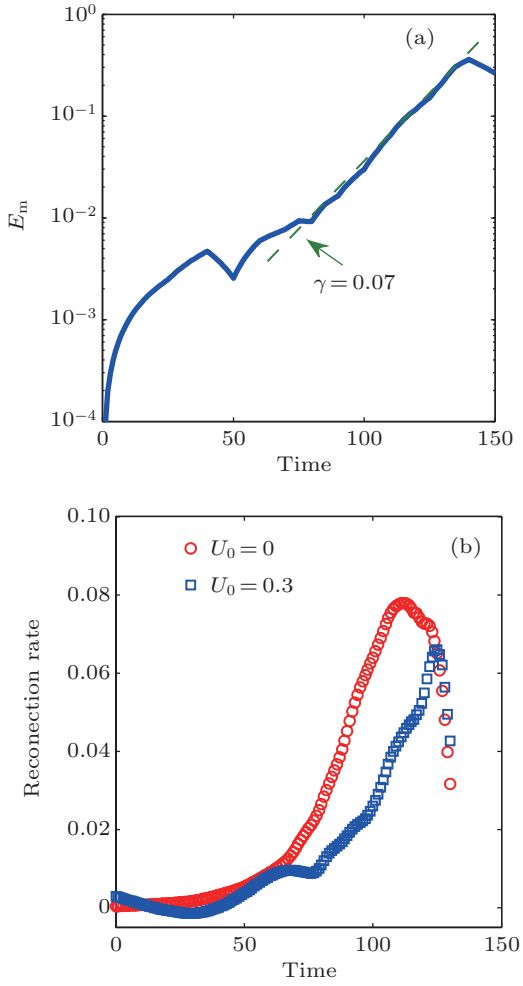


Fig. 5. (color online) Growth rates of reconnection in Case II. Panel (a) shows the temporal evolution of magnetic energy E_m, with the slope (green dash line) representing the growth rate of $\gamma = \mathrm{d}(\ln E_m)/\mathrm{d}t \approx 0.07$, and panel (b) shows the temporal evolutions of $E_y = \partial\psi/\partial t$ for reconnection processes without shear flow ($U_0 = 0$) and with shear flow ($U_0 = 0.3V_A$).

4. Effects of flows with shear in *x* direction

The out-of-plane (toroidal) shear flow discussed in Section 3 is a "z-dependent" equilibrium flow. Generally speaking, for a 2D "toroidal" shear flow $u_y = u_y(x,z)$ in a Harris sheet, the $\boldsymbol{u}_0 \times \boldsymbol{B}_0 = -\hat{z}u_{y0}(x,z)B_{x0}(z)$. If the out-of-plane flow is $u_y = u_y(z)$ as in Section 3, we always have $\nabla \times (\boldsymbol{u}_0 \times \boldsymbol{B}_0) = 0$, satisfying the Harris sheet equilibrium. Nevertheless, for the general 2D out-of-plane flow $u_y = u_y(x,z)$, we can have $\nabla \times (\boldsymbol{u}_0 \times \boldsymbol{B}_0) = \hat{y}B_{x0}\partial u_y/\partial x \neq 0$. Then, the initial out-of-plane flow $u_y = u_y(x,z)$ can immediately generate an out-of-plane magnetic field B_y to reduce or enhance the out-of-plane Hall field. Thus, in this section we will further discuss the out-of-plane "driven" flow effect with an "x-dependence". In a way similar to that in Section 3, flows, symmetric and antisymmetric about the z axis are imposed on the Harris sheet equilibrium.

4.1. Effect of symmetric flows varied in *x* direction (Case III)

The flow symmetric about z axis is assumed to be

$$u_{iy0}(x) = U_0 \exp\left(-x^2/L_s^2\right), \tag{17}$$

which is shown in Fig. 1(c) and here indicated as Case III.

In Fig. 6, the configuration of the magnetic flux, the color contour plot of the out-of-plane magnetic field component, and the corresponding out-of-plane vorticity $\omega_y(x,z)$ together with the in-plane flow pattern, which is shown by arrows, and the plasma density distribution are plotted, respectively, at $t = 125\tau_A$ and for $U_0 = 0.3V_A$.

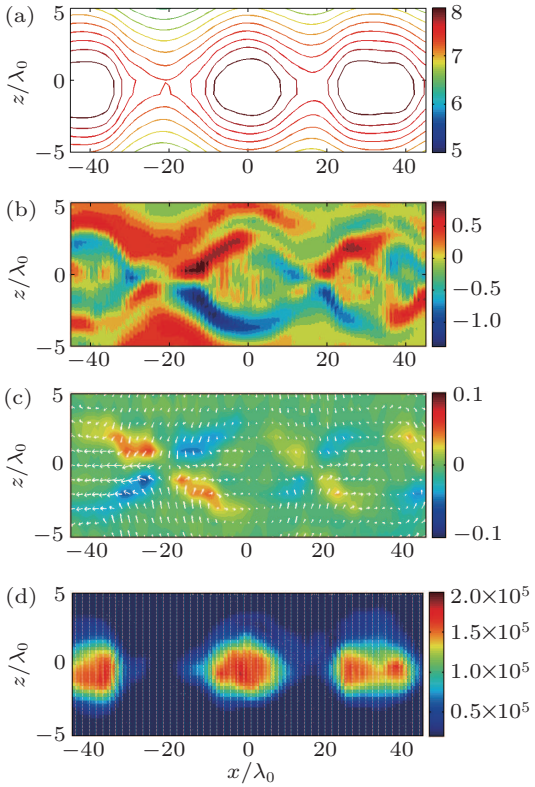


Fig. 6. (color online) Effects of the shear flows given by Eq. (17) with $U_0 = 0.3V_A$ and at $t = 125\tau_A$. Panel (a) shows the configuration of the in-plane magnetic flux, panel (b) shows the distribution of the out-of-plane magnetic field B_y, panel (c) shows the distributions of the out-of-plane vorticity ω_y (in contours) and the in-plane flows $\boldsymbol{u}_x + \boldsymbol{u}_z$ (in arrows), and panel (d) shows the density of plasma.

Dramatic changes of the out-of-plane magnetic field and vorticity due to the shear flow are seen in Fig. 6. As shown previously,[27,28] a quadrupolar structure of $B_y^{(S)}$ can be generated by the out-of-plane symmetric flow with its shear along the initial neutral line ($z = 0$). As the flow strength U_0 increases, for example, $U_0 = 0.3V_A$, it is clearly indicated that the flow generated quadrupolar structure $B_y^{(S)}$ is of the same order of the Hall effect generated quadrupolar structure $B_y^{(H)}$, i.e., $B_y^{(S)} \sim B_y^{(H)}$. It has been found that, if $U_0 > 0$, then the shear flow generated quadrupolar structure $B_y^{(S)}$ is opposite to $B_y^{(H)}$.[27] In the case of $U_0 = 0.3V_A$, we have $|B_y^{(S)}| > |B_y^{(H)}|$, which then eliminates the Hall quadrupolar field structure and

reverses the reconnection process around the origin ($x = z = 0$) by turning the X-point at the point to an O-point. However, since the flow distribution is localized only in a small region of $|x| \sim L_s = 4$, the reconnection process still occurs in the plasma to form another two X-points, near $x \sim \pm 20$, and Hall quadrupolar field structures form around them. It can, therefore, be seen as a "multiple X-points" reconnection process. The growth of the "multiple X-points" island is shown in Fig. 7.

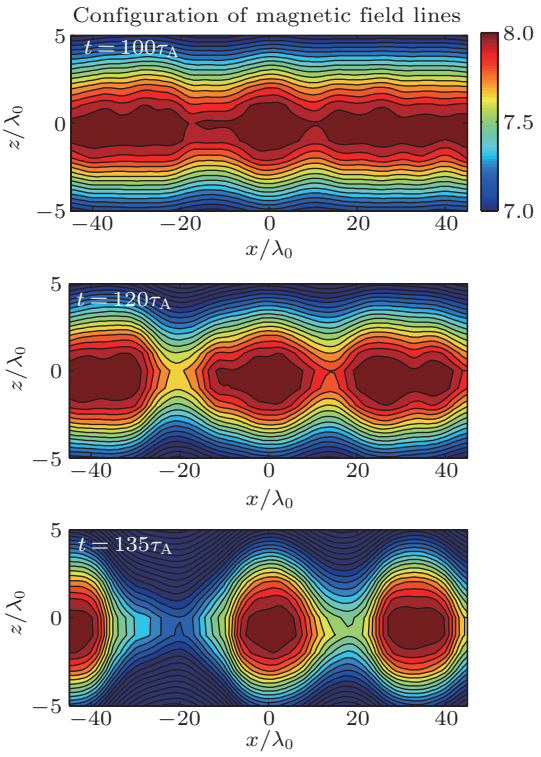


Fig. 7. (color online) Growths of the "micro-islands".

The temporal evolutions of the magnetic energy E_m for $U_0 = 0.3V_A$, together with the reconnection rate, $\partial\psi/\partial t$, are then shown in Fig. 8. In Fig. 8(a), which is calculated by using the slope of the E_m growth, the reconnection rate is found to be approximately 0.08, i.e., $\gamma \approx 0.08$, which is in a reasonable agreement with $\gamma \approx 0.07$ shown in Fig. 8(b) for the growth rate at one of the X-points, while the reconnection rate at the origin (an O-point) is approximately kept vanished.

On the contrary, if $U_0 < 0$, the flow can generate a quadrupole field parallel to $B_y^{(H)}$, and enhance the reconnection rate at the origin. Fig. 9 shows how the reconnection rate at the origin varies with the strength of the shear flow U_0. For $U_0 < 0$, if the strength is negative enough, for example, $U_0 = -0.2$, then the reconnection rate is significantly enhanced to $\gamma \approx 0.13$. As U_0 increases to the positive regime ($U_0 > 0$), the reconnection rate at the origin becomes reduced. Then, the X-point turns into an O-point at the origin to trigger "multiple X-points" reconnection.

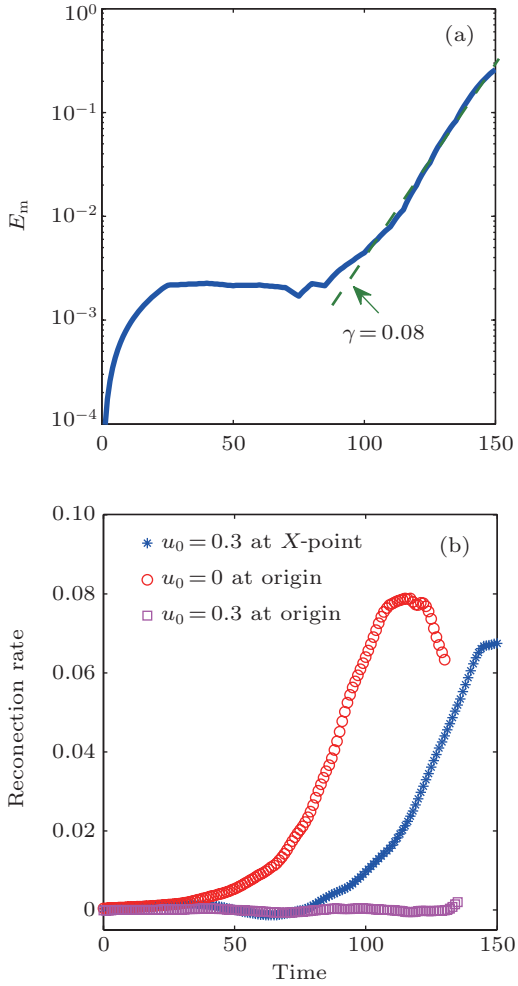


Fig. 8. (color online) Growth rates of reconnection in Case III. Panel (a) shows the temporal evolution of magnetic energy E_m, with the slope (green dash line) representing the growth rate of $\gamma = \mathrm{d}(\ln E_m)/\mathrm{d}t \approx 0.08$, panel (b) shows the temporal evolutions of $E_y = \partial\psi/\partial t$ for reconnection processes without shear flow ($U_0 = 0$) and with shear flow ($U_0 = 0.3V_A$) at the origin (pink squares) and at the X-point (blue stars).

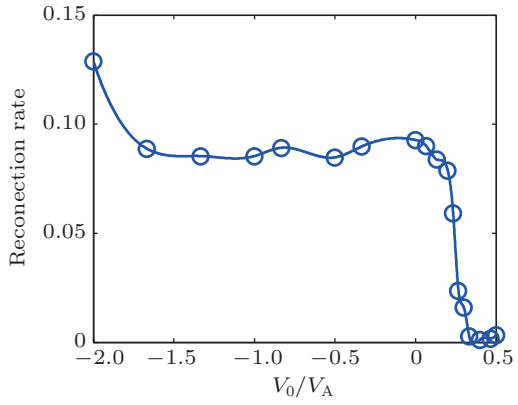


Fig. 9. (color online) Reconnection rate at the origin as a function of strength of shear flow.

4.2. Effect of antisymmetric flows varied in x direction (Case IV)

The antisymmetric flow with a shear in the x direction is given by

$$u_{\mathrm{iy0}}(x) = U_0 \tanh\left(x/L_{\mathrm{S}}\right), \tag{18}$$

as shown in Fig. 1(d), with also $U_0 = 0.3$.

The configuration of the magnetic flux, the color contour plot of the out-of-plane magnetic field component, and the corresponding out-of-plane vorticity $\omega_y(x,z)$, together with the $\boldsymbol{u}_x + \boldsymbol{u}_z$ pattern denoted with arrows, and the plasma density distribution are again plotted, respectively, in Figs. 10(a)–10(d), at $t = 115\tau_{\mathrm{A}}$ and for $U_0 = 0.3V_{\mathrm{A}}$. The solid vertical line in Fig. 10(a) indicates the origin and the dashed vertical line marks the X-point due to the shear flow effect. "Secondary" islands can also be seen in the process.

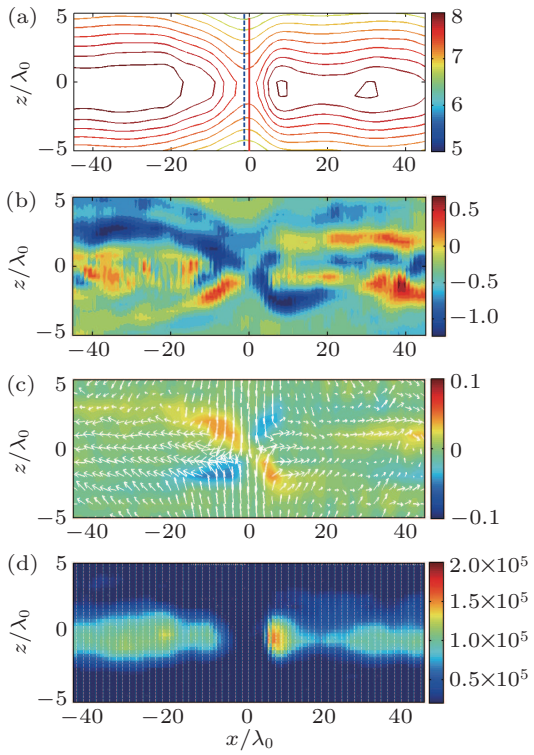


Fig. 10. (color online) Effects of the shear flows given by Eq. (18) with $U_0 = 0.3V_{\mathrm{A}}$ and at $t = 115\tau_{\mathrm{A}}$. Panel (a) shows the configuration of the in-plane magnetic flux, panel (b) shows the distribution of the out-of-plane magnetic field B_y, panel (c) shows the distributions of the out-of-plane vorticity ω_y in contours and the in-plane flows $\boldsymbol{u}_x + \boldsymbol{u}_z$ (in arrows), and panel (d) shows the density of plasma.

The temporal evolutions of the magnetic energy E_{m} for this case, and the reconnection rate, $\partial\psi/\partial t$, are shown in Figs. 11(a) and 11(b). In Fig. 11(a), which is calculated by using the slope of the E_{m} growth, the reconnection rate is found to be approximately 0.09; that is, $\gamma \approx 0.09$. As shown in Fig. 11(b) the reconnection rate, $\partial\psi/\partial t$ at the shifted X-point is approximately the same as that in Fig. 11(a). Therefore, such an X-point shift does not have a substantial effect on the major reconnection. Nevertheless, a couple of "micro-islands" can be found in the process (Fig. 10(a)).

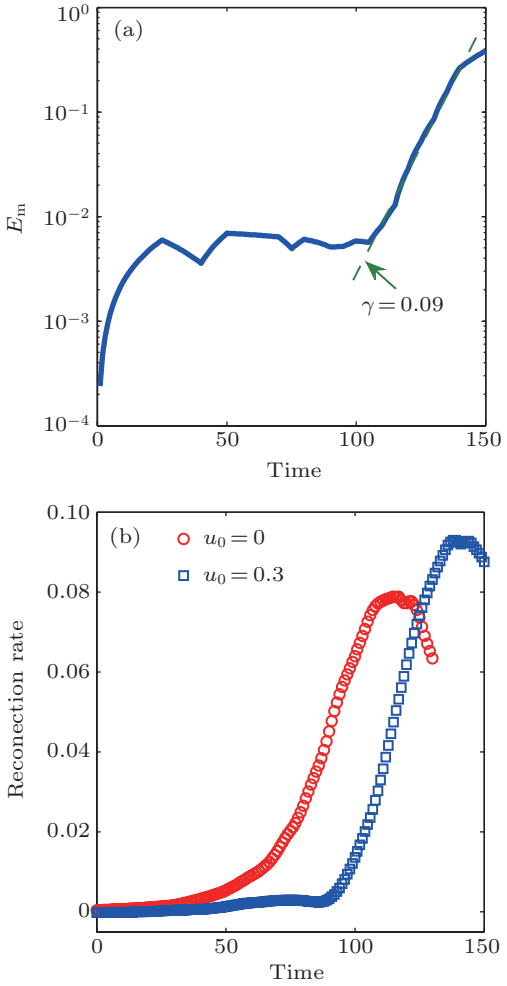


Fig. 11. (color online) Growth rates of reconnection in Case IV. Panel (a) shows the temporal evolution of magnetic energy E_{m}, with the slope (green dash line) representing the growth rate of $\gamma = \mathrm{d}\left(\ln E_{\mathrm{m}}\right)/\mathrm{d}t \approx 0.09$, and panel (b) shows the temporal evolutions of $E_y = \partial\psi/\partial t$ for reconnection processes without shear flow ($U_0 = 0$) and with shear flow ($U_0 = 0.3V_{\mathrm{A}}$).

5. Discussion and summary

In this paper we discuss the effects of out-of-plane shear flows on magnetic reconnection in 2D hybrid simulations, for various symmetric or antisymmetric flow profiles.

It is found in previous studies that an out-of-plane magnetic field component can be generated by the out-of-plane shear flow even without Hall effect in a 2D resistive MHD model.[28] It has also been shown in the Hall MHD model that the out-of-plane magnetic field component induced by shear flow can be coupled to Hall effect.[27] If the flow shear is strong enough, the quadrupole field generated by Hall effect can be significantly distorted.

An important feature of the Hall effect in magnetic reconnection is to generate quadrupolar structure of out-of-plane magnetic field component, called the Hall quadrupolar field, which is also seen in observations and laboratory experiments. Thus, this out-of-plane quadrupole field perturbation is usually taken as the main signature of a Hall MHD magnetic reconnection regime. Nevertheless, previous studies have shown that the out-of-plane shear flows may significantly affect the

signature.[27,28]

In this paper we use four various shear flow profiles varying in-plane, which are the same as those in Ref. [27], in a 2D hybrid model to further study the effect of out-of-plane shear flow on fast magnetic reconnection. The shear flow in each case is imposed on the initial equilibrium state, and the result is compared with that in the case without the shear flow.

The results obtained in the present study can be summarized as follows.

(i) For the equilibrium shear flow varying in the direction of initial magnetic shear (i.e., the z direction) the effect of the symmetric flow on the reconnection process is not substantial, while the effect of the antisymmetric flow, particularly on the out-of-plane magnetic field pattern (shown in Fig. 4) is obvious.

(ii) For the "driven" shear flow varying in the direction of initial magnetic field (i.e., the x direction) the effect of the symmetric flow on the reconnection process is significant. The initial symmetric point, the origin in the configuration discussed, turns into an O-point instead of an X-point in other cases. Consequently, a "multiple X-points" reconnection process is triggered.

(iii) For the antisymmetric "driven" shear flow varying in the x direction, the effect of the flow is also observable. Although it does not affect the major reconnection process much, one can clearly see the formation of "micro-islands", which may be helpful in understanding the "secondary islands" observed in magnetotail plasmas.

References

[1] Biskamp D 2000 *Magnetic Reconnection in Plasmas* (New York: Cambridge University Press) p. 1–4
[2] Priest E and Forbes T 2000 *Magnetic Reconnection: MHD Theory and Applications* (New York: Cambridge University Press) p. 1–6
[3] Birn J, Gosling J T, Hesse M, Forbes T G and Priest E R 2000 *Astrophys. J.* **541** 1078
[4] Lazarian A and Vishniac E T 1999 *Astrophys. J.* **517** 700
[5] Yamada M, Kulsrud R and Ji H 2010 *Rev. Mod. Phys.* **82** 603
[6] Guo J, Yu B, Guo G H and Zhao B 2011 *Chin. Phys. Lett.* **28** 025201
[7] Ma Z W and Feng S L 2008 *Chin. Phys. Lett.* **25** 2934
[8] Huang J and Ma Z W 2008 *Chin. Phys. Lett.* **25** 1764
[9] Guo J and Lu Q M 2007 *Chin. Phys. Lett.* **24** 3199
[10] Guo J, Lu Q M, Wang S and Fu X R 2005 *Chin. Phys. Lett.* **22** 409
[11] Jensen T H and Leonard A W 1991 *Phys. Fluid B* **3** 3422
[12] Wang X and Bhattacharjee A 1992 *Phys. Fluid B* **4** 1795
[13] Luan Q B, Shi Y P and Wang X G 2012 *Chin. Phys. Lett.* **29** 085201
[14] Ma Z W, Ng C S, Wang X G and Bhattacharjee A 1995 *Phys. Plasmas* **2** 3184
[15] Ma Z W, Wang X and Bhattacharjee A 1996 *Phys. Plasmas* **3** 2427
[16] Liu C G and Qian S J 1998 *Acta Phys. Sin.* (Overseas Edition, i.e., Chin. Phys.) **7** 22
[17] Wang X and Bhattacharjee A 1997 *Phys. Plasmas* **4** 748
[18] Zhang Y and Ding N 2008 *Chin. Phys. B* **17** 2994
[19] Wei L and Wang Z X 2011 *Nucl. Fusion* **51** 123005
[20] Shen C and Liu Z X 1996 *Phys. Plasmas* **3** 4301
[21] Xu T, Hu Q M, Hu X W and Yu Q Q 2011 *Chin. Phys. Lett.* **28** 095202
[22] La Belle-Hamer A L, Otto A and Lee L C 1994 *Phys. Plasmas* **1** 706
[23] Nakamura R, Baumjohann W, Nagai T, Fujimoto M, Mukai T , Klecker B, Treumann R, Balogh A, Rème H, Sauvaud J A, Kistler L, Mouikis C, Owen C J, Fazakerley A N, Dewhurst J P and Bogdanova Y 2004 *J. Geophys. Res.* **109** A05204
[24] Lin Y and Lee L C 1994 *Geophys. Res. Lett.* **21** 855
[25] La Belle-Hamer L A, Otto A and Lee L C 1995 *J. Geophys. Res.* **100** 11875
[26] Sun X X, Lin Y and Wang X G 2005 *Phys. Plasmas* **12** 012305
[27] Wang J Q, Xiao C J and Wang X G 2012 *Phys. Plasmas* **19** 032905
[28] Wang J Q, Wang X G and Xiao C J 2008 *Phys. Lett. A* **372** 4614
[29] Swift D W 1995 *Geophys. Res. Lett.* **22** 311
[30] Lin Y and Swift D W 1996 *J. Geophys. Res.* **101** 19859
[31] Yin L, Winske D, Gary S P and Birn J 2001 *J. Geophys. Res.* **106** 10761
[32] Wang X Y, Lin Y and Chang S W 2009 *J. Geophys. Res.* **114** A06203
[33] Yamada M, Ren Y, Ji H, Breslau J, Gerhardt S, Kulsrud R and Kuritsyn A 2006 *Phys. Plasmas* **13** 052119
[34] Ren Y, Yamada M, Gerhardt S, Ji H, Kulsrud R and Kuritsyn A 2005 *Phys. Rev. Lett.* **95** 055003
[35] Wang X, Bhattacharjee A and Ma Z W 2001 *Phys. Rev. Lett.* **87** 265003
[36] Wang X, Bhattacharjee A and Ma Z W 2000 *J. Geophys. Res.* **105** 27633
[37] Ding W X, Brower D L, Craig D, Deng B H, Fiksel G, Mirnov V, Prager S C, Sarff J S and Svidzinski V 2004 *Phys. Rev. Lett.* **93** 045002